energies

MDPI

Article

Evaluation of Recovery of Tight Sandstone Gas Reservoirs Based on a Seepage Steady-State Model

Jianzhong Zhang [1,2,3,*], Shusheng Gao [1,2,3], Wei Xiong [1,2,3], Liyou Ye [1,2,3], Huaxun Liu [2], Wenqing Zhu [2], Weiguo An [2], Donghuan Han [1,2,3] and Baicen Lin [1,2,3]

[1] University of Chinese Academy of Sciences, Beijing 101408, China; handonghuan19@mails.ucas.edu.cn (D.H.)
[2] Institute of Porous Flow & Fluid Mechanics, Chinese Academy of Sciences, Langfang 065007, China
[3] Research Institute of Petroleum Exploration and Development, Beijing 100083, China
* Correspondence: zhangjianzhong19@mails.ucas.edu.cn

Abstract: As an important indicator for measuring the effectiveness and level of oil and gas field development, recovery rate has always been a focus in the research of oil and gas fields. Reservoirs of tight sandstone gas formations have significant characteristics of low porosity, high permeability, and high water content, which leads to greater difficulty in their development and makes it challenging to evaluate the recovery rate. Newtonian mechanics, as an important component of the mechanical system, is an innovative application of classical mechanics in the field of seepage mechanics when applied to the two-phase flow of gas and water. Firstly, starting from the perspective of mechanics analysis, we derive a steady-state model for gas–water two-phase infiltration and obtain the productivity equation based on this model. Then, according to the steady-state model, we establish a method to calculate the effective control radius of gas reservoirs under different production conditions and reservoir physical properties. Finally, using Matlab 2018a programming based on the productivity equation, we calculate the gas recovery under different conditions during constant pressure drop production and constant production rate production. The results indicate that the effective control radius of the reservoir decreases with an increase in the economic ultimate daily gas production, increases with an increase in production pressure difference, slightly decreases with an increase in startup pressure gradient, and correspondingly increases with an increase in microtube radius and quantity. Regardless of whether it is production with a fixed pressure drop or production with a fixed production rate, the gas recovery decreases as the production pressure drop and bottomhole abandonment pressure increase, but it increases as the proportion of the single-well control radius increases. In production with a fixed pressure drop, the gas recovery remains consistent across different reservoir quality indices. However, in production with a fixed production rate, the gas recovery initially increases rapidly and then gradually slows down as the reservoir quality index increases, and there is an obvious critical permeability (0.1 mD). The research findings are based on the mechanical analysis of porous media, delving into the laws governing fluid flow during infiltration. The derived infiltration model can be used to calculate the effective control radius and evaluate recovery rates, providing practical guidance for reservoir development.

Keywords: seepage steady-state model; productivity equation; effective control radius; gas recovery

check for updates

Citation: Zhang, J.; Gao, S.; Xiong, W.; Ye, L.; Liu, H.; Zhu, W.; An, W.; Han, D.; Lin, B. Evaluation of Recovery of Tight Sandstone Gas Reservoirs Based on a Seepage Steady-State Model. *Energies* **2024**, *17*, 1421. https://doi.org/10.3390/en17061421

Academic Editor: Reza Rezaee

Received: 16 February 2024
Revised: 12 March 2024
Accepted: 12 March 2024
Published: 15 March 2024

Copyright: © 2024 by the authors. Licensee MDPI, Basel, Switzerland. This article is an open access article distributed under the terms and conditions of the Creative Commons Attribution (CC BY) license (https://creativecommons.org/licenses/by/4.0/).

1. Introduction

Recovery is the most important comprehensive index to measure the development effect and level of oil and gas fields, and it is also one of the key issues in the dynamic analysis of oil and gas fields [1–4]. Tight sandstone gas reservoirs are characterized by low porosity, low permeability, and high water saturation [5,6], which makes it difficult to develop them, and there are many influencing factors and complex influencing mechanisms [7,8]. Therefore, the study of recovery evaluation for tight sandstone gas reservoirs

is of great guiding significance for the efficient development of gas reservoirs, and it is helpful to understand and evaluate the recovery level of gas reservoirs.

For many years, the research on recovery of gas reservoirs has been continuous. There are various calibration methods for recovery of tight sandstone gas reservoirs, including the empirical method [9], material balance method [3], modified pressure drop method [10], production decline method [11], Rogersti function method [12], analog method [13], etc. Improving the recovery of gas reservoirs has always been a hot topic of concern among scholars and experts around the world. The main methods to improve the recovery of tight sandstone gas reservoirs include reservoir fracturing and reconstruction technology [14,15], well pattern encryption technology [16–18], surface pressurization technology [19,20], and increasing the ultimate economic production [21].

Based on Newton's law of motion, this paper deduces the steady-state model of gas–water two-phase seepage and its corresponding productivity equation by means of mechanical analysis. Then, on the basis of the steady-state model, the calculation method of effective production radius of tight sandstone gas reservoir is established, and the effective production radius is calculated under different production and reservoir physical properties. Finally, according to the productivity equation, gas recovery under different conditions of constant pressure difference production and constant output production is calculated by the Matlab programming method, and an example is calculated.

2. Steady-State Model of Gas–Water Two-Phase Seepage in a Tight Sandstone Gas Reservoir

2.1. Establishment of a Steady-State Model of Gas–Water Two-Phase Seepage

A micropipe with length L and radius R was analyzed by force, and a steady-state mechanical model of gas–water two-phase seepage was established, as shown in Figure 1. The model considers the existence of water film and assumes that the whole process is carried out under the condition of hydraulic smoothness; that is, wall roughness does not affect the flow process.

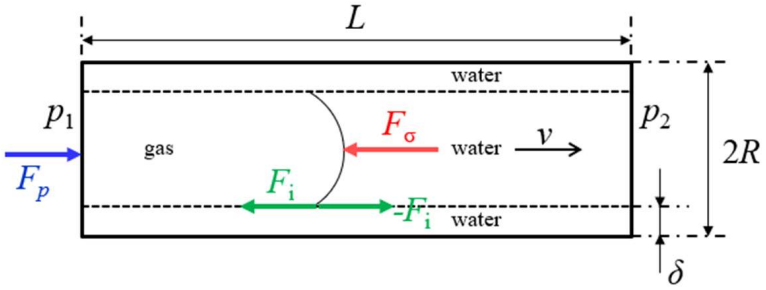

Figure 1. Steady-state mechanical model of gas–water two-phase seepage.

In the figure, F_p is the displacement force caused by the pressure difference, in N; F_σ is the capillary force [22], in N; F_i is the internal friction force, in N; R is the radius of the pipeline, in m; δ is the thickness of the water film, in m; L is the length of the pipeline, in m; and v is the velocity, in $\mathrm{m{\cdot}s^{-1}}$.

The force of gas–water two-phase seepage under a steady-state condition reaches equilibrium, as follows:

$$\pi(R-\delta)^2 \cdot \Delta p - 2\pi(R-\delta)\sigma\cos\theta - 2\pi(R-\delta)L \cdot \tau = 0 \quad (1)$$

where Δp is the displacement pressure difference, in Pa; σ is the interfacial tension, in $\mathrm{N{\cdot}m^{-1}}$; θ is the contact angle, in rad; and τ is the shear stress, or the internal friction force per unit area, in $\mathrm{N{\cdot}m^{-2}}$, that is:

$$\tau = -\mu\frac{du_r}{dr} \quad (2)$$

where r is the radius of the circle, in m, and u_r is the velocity at radius r, in $\mathrm{m{\cdot}s^{-1}}$.

From Equation (1), the following can be obtained:

$$\tau = -\mu\frac{du_r}{dr} = \frac{1}{2L}[\Delta p(R-\delta) - 2\sigma cos\theta] \tag{3}$$

The water film does not participate in the flow, and the fluid velocity on the surface of the water film is 0, that is, when $r = R - \delta$, $u_r = 0$. Integrating both sides of the above formula, the radius is anywhere from r to $R - \delta$, and the velocity is from u_r to 0, that is:

$$u_r = \frac{\Delta p}{4\mu L}\left[(R-\delta)^2 - r^2\right] - \frac{\sigma\cos\theta(R-\delta-r)}{\mu L} \tag{4}$$

The average velocity is:

$$u = \frac{1}{A}\iint u_r dA = \frac{\Delta p(R-\delta)^2}{8\mu L} - \frac{\sigma cos\theta(R-\delta)}{3\mu L} \tag{5}$$

The Equation (5) above shows the relationship between the velocity and pressure difference, pipe radius, water film thickness, viscosity, etc. under the condition of force balance, which is a steady-state model of gas–water two-phase seepage derived from mechanical analysis.

2.2. Productivity Equation Based on a Gas–Water Two-Phase Seepage Steady-State Model

For a circular, homogeneous constant pressure boundary formation of the same thickness (Figure 2), if the gas well is produced at a fixed rate, the gas flow can reach a stable state.

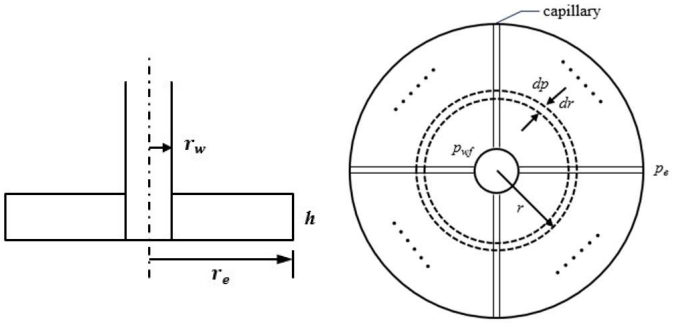

Figure 2. Circular, homogeneous constant pressure boundary formation of the same thickness.

In the figure, r is the radius of any point from the center point of the gas well, in m; r_w is the completion radius, in m; r_e is the radius of the outer boundary, in m; h is the formation thickness, in m; p_{wf} is the bottom hole pressure, in Pa; and p_e is the outer formation boundary pressure, in Pa.

Supposing that in a circular, homogeneous constant pressure boundary formation of the same thickness, N capillary tubes with radius R and length $r_e - r_w$ are distributed along the circumference of the formation (Figure 2), and the porosity is as follows:

$$\phi = \frac{N\pi R^2(r_e - r_w)}{(\pi {r_e}^2 - \pi {r_w}^2)h} \tag{6}$$

According to Equation (5), the flow rate in a single tube can be determined as:

$$q = \pi(R-\delta)^2 u = \frac{\pi(R-\delta)^4\Delta p}{8\mu(r_e - r_w)} - \frac{\pi(R-\delta)^3\sigma\cos\theta}{3\mu(r_e - r_w)} \tag{7}$$

Thus, the flow rate in the whole formation is:

$$Q = Nq = N\left[\frac{\pi(R-\delta)^4}{8\mu}\frac{dp}{dr} - \frac{\pi(R-\delta)^3\sigma\cos\theta}{3\mu(r_e - r_w)}\right] \tag{8}$$

The flow rate of ground conditions is:

$$Q_{sc} = \frac{Q}{B_j} = \frac{\phi\left(\pi {r_e}^2 - \pi {r_w}^2\right)h}{\pi R^2(r_e - r_w)} \cdot \frac{T_{sc}Z_{sc}p}{TZp_{sc}}\left[\frac{\pi(R-\delta)^4}{8\mu}\frac{dp}{dr} - \frac{\pi(R-\delta)^3\sigma\cos\theta}{3\mu(r_e - r_w)}\right] \tag{9}$$

where Q_{sc} is the total flow of ground conditions, in $m^3 \cdot s^{-1}$; B_j is the volume coefficient; and T_{sc} is the temperature in the standard state, the unit is K, and the value is 273.15. Z_{sc} is the deviation factor in the standard state, and the value is 1. T is the current temperature, in K; Z is the deviation factor under current pressure; and p_{sc} is the standard pressure, that is, atmospheric pressure, the unit is Pa, and the value is 0.101×10^6.

Considering the influence of pressure on the deviation factor and viscosity, let $a = \frac{\phi\left(\pi {r_e}^2 - \pi {r_w}^2\right)h}{\pi R^2(r_e - r_w)}\frac{T_{sc}Z_{sc}}{TZp_{sc}}\frac{\pi(R-\delta)^4}{8\mu}$, $b = -\frac{\phi\left(\pi {r_e}^2 - \pi {r_w}^2\right)h}{\pi R^2(r_e - r_w)}\frac{T_{sc}Z_{sc}}{TZp_{sc}}\frac{\pi(R-\delta)^3\sigma\cos\theta}{3\mu(r_e - r_w)}$. The influence of the deviation factor and viscosity is considered in the coefficients a and b, and the pressure range is selected in stages during calculation to ensure that the deviation factor and viscosity change in a single pressure range is minimal, and the deviation factor and viscosity are calculated separately for each pressure range. Equation (9) can be simplified as:

$$Q_{sc} = a \cdot p\frac{dp}{dr} + b \cdot p \tag{10}$$

Sorting can obtain:

$$a \cdot pdp + (b \cdot p - Q_{sc})dr = 0 \tag{11}$$

The above equation is a first-order ordinary differential equation with separable variables. Dividing both sides by $(bp - Q_{sc})$, we get:

$$\frac{a \cdot p}{b \cdot p - Q_{sc}}dp + dr = 0 \tag{12}$$

Integrating along the radial distance (from completion distance r_w to anywhere r), we get:

$$\frac{aQ_{sc}}{b^2}\ln^{\frac{bp - Q_{sc}}{bp_{wf} - Q_{sc}}} + \frac{a}{b}\left(p - p_{wf}\right) + (r - r_w) = 0 \tag{13}$$

At the outer boundary, we get:

$$\frac{aQ_{sc}}{b^2}\ln^{\frac{bp_e - Q_{sc}}{bp_{wf} - Q_{sc}}} + \frac{a}{b}\left(p_e - p_{wf}\right) + (r_e - r_w) = 0 \tag{14}$$

Equation (14) is the calculated productivity equation derived from the steady-state model, and the relationship between flow rate and bottom-hole flow pressure can be obtained by solving Equation (14).

3. Effective Control Radius of a Tight Sandstone Gas Reservoir

The key to effective development of tight sandstone gas reservoirs is to determine reasonable well pattern density and effective development well spacing of gas reservoirs based on the effective control radius of the gas reservoir and comprehensive consideration of technical, economic, and other factors [23,24]. Therefore, the analysis of the fluid flow process in a gas reservoir and the determination of the effective control radius have important guiding significance for the deployment of a gas reservoir development well pattern.

The process of pressure propagation in the reservoir is shown in Figure 3 [25]. With the increase in production time, formation pressure gradually decreases, pressure waves con-

stantly propagate outward from well point A, and the reservoir utilization scope gradually increases, but the driving pressure gradient gradually decreases.

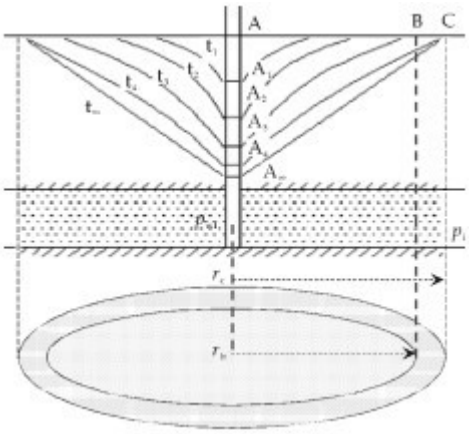

Figure 3. Pressure wave propagation process in reservoir [25].

In the reservoir, the pressure gradient at the radius r_c (C in Figure 3) is less than the starting pressure gradient, so that the seepage velocity $v = 0$, and the radius r_c is the limit control radius. The limit control radius usually refers to the leakage radius corresponding to the zero-seepage velocity in the reservoir under the given pressure difference condition [26]. The development well spacing determined by the limit control radius has some problems in actual production. On the one hand, when the pressure wave propagates to the boundary, the gas well production is already below the economic daily gas limit, and the well has to be shut in, effectively making the reserves in the area near the boundary impossible to use. On the other hand, even if the shut-in limit is very low to meet the pressure wave propagation to the limit control radius, the overall pressure drop in the area near the boundary is also small, so the degree of reserve exploitation in this part is also very low.

In the actual production and development, the fluid near the boundary of the reservoir must also have a certain seepage speed, so that when the pressure wave is transmitted here, it also has a certain output, which can meet the requirements of the production limit of the gas well. Therefore, the actual development well spacing should be less than the limit control radius, that is, the effective control radius, as shown by B in Figure 3.

The effective control radius of the reservoir is actually the maximum development well distance that the gas reservoir can benefit from economically under certain development conditions. Under the given gas reservoir physical property conditions and determined production pressure difference, the control radius r_b, corresponding to the economic limit of daily production Q_m, is the effective control radius of the reservoir.

In the circular uniform thickness constant pressure boundary formation model shown in Figure 2, Equation (5) is rewritten into polar coordinate form, that is:

$$u = \frac{(R-\delta)^2}{8\mu}\frac{dp}{dr} - \frac{\sigma\cos\theta(R-\delta)}{3\mu}\cdot\frac{1}{r} \tag{15}$$

Considering the starting pressure gradient, Equation (15) becomes:

$$u = \frac{(R-\delta)^2}{8\mu}\left(\frac{dp}{dr} - G\right) - \frac{\sigma\cos\theta(R-\delta)}{3\mu}\cdot\frac{1}{r} \tag{16}$$

where G is the starting pressure gradient, in MPa·m^{-1}.

The flow rate throughout the formation is:

$$Q = Nq = N\left[\frac{\pi(R-\delta)^4}{8\mu}\left(\frac{dp}{dr} - G\right) - \frac{\pi(R-\delta)^3\sigma\cos\theta}{3\mu}\cdot\frac{1}{r}\right] \tag{17}$$

The pressure gradient is:

$$\frac{dp}{dr} = \frac{8\mu Q}{N\pi(R-\delta)^4} + \frac{8\sigma\cos\theta}{3(R-\delta)} \cdot \frac{1}{r} + G \tag{18}$$

The pressure distribution expression can be obtained from Equation (18) as follows:

$$p(r) = p_w + \left[\frac{8\mu Q}{N\pi(R-\delta)^4} + G\right](r - r_w) + \frac{8\sigma\cos\theta}{3(R-\delta)} \cdot \ln\frac{r}{r_w} \tag{19}$$

The specific steps for calculating the propagation range of pressure waves are as follows:

(1) Determine the initial conditions, take the bottom of the gas well as the starting point, and gradually extrapolate for iterative calculation. The fitting time t_i starts from 0, 1, . . . , t_m, . . . , t_n changes. The corresponding pressure wave propagates outward gradually, and the control radius increases gradually.

(2) Determine the initial radius increment Δr, calculate the effective propagation range of the pressure wave, and calculate the change of the pressure distribution within the range.

(3) At a certain time t_i, the corresponding propagation distance, that is, the control radius, is $t_i \cdot \Delta r$, and the gas well production and displacement pressure gradient corresponding to the control radius are calculated.

(4) Judge the situation of the t_i moment to determine whether the displacement pressure gradient at the pressure wave propagation is greater than the starting pressure gradient. If so, increase the pressure propagation distance and continue the iterative calculation. If not, reduce the radius increment Δr.

(5) When the production reaches a certain time t_m, the pressure wave propagates to a place r_b in the formation, where the displacement pressure gradient is greater than the starting pressure gradient, and the pressure wave can continue to propagate outward. When the gas well production Q is equal to the economic limit of daily gas production Q_m, the corresponding r_b is the effective control radius of the reservoir.

Sulige gas field is a typical tight sandstone gas reservoir. A well was selected as an example for analysis. The basic parameters are shown in Table 1 below.

Table 1. Basic data sheet of a gas well.

Pound Sign	Reservoir Thickness/m	Permeability/mD	Completion Radius/m	Porosity/%	Gas Saturation/%
X	20.7	0.156	0.1	8.83	61.69

The initial economic limit of the gas reservoir is set at 1.5 $m^3 \cdot d^{-1}$. The shut-in daily production limit is the production rate at which the daily production revenue (sales revenue per day) of the gas well is equal to the daily production expenditure of the gas well.

Based on the theoretical basis of Equations (15)–(19), taking the basic data of X gas well in Sulige gas field as an example, the above calculation methods and steps were used to study the distribution law of reservoir displacement pressure gradient under different conditions, and the effective control radius of the gas well was determined according to the economic limit of shut-in daily gas production.

Under the conditions of different production pressure differences and start-up pressure gradients with given reservoir physical property conditions, the displacement pressure gradient distribution law within the reservoir production range is shown in Figure 4 below.

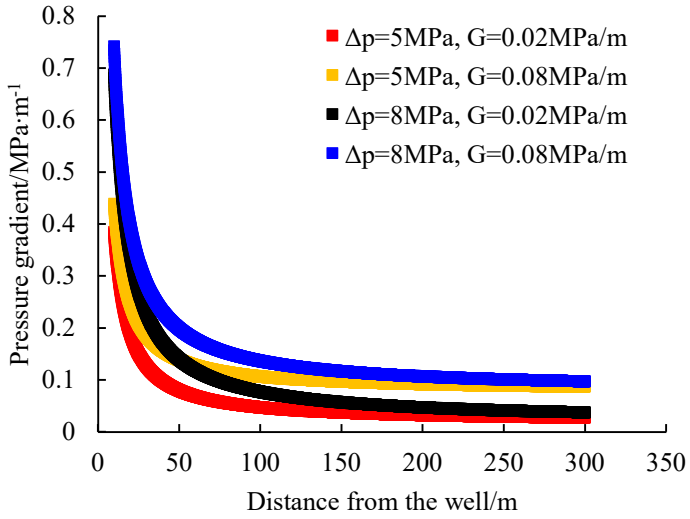

Figure 4. Distribution of displacement pressure gradient under different conditions.

As can be seen from Figure 4, under certain production pressure differential conditions, the displacement pressure gradient within the range of operation increases with the increase in the starting pressure gradient. Under a certain starting pressure gradient condition, the larger the production pressure difference, the larger the displacement pressure gradient in the range of production. Especially in the pre-production area near the well, the difference is more obvious, and the variation range of the displacement pressure gradient in the range of production also increases with the increase in the production pressure difference.

With the progress of gas well production, the pressure wave gradually propagates outward, and the gas well production gradually decreases. When the gas well production reaches the economic limit of daily gas production Q_m, the corresponding control radius is the effective control radius of the reservoir. When gas well production $Q = 0$, the corresponding control radius is the limit control radius. Under different production conditions, the effective control radius of the reservoir is smaller than the limit control radius under the same condition.

Given the starting pressure gradient of 0.05 MPa·m^{-1}, the relationship between the effective control radius of the reservoir and the economic limit of daily gas production under different production pressure differential conditions is shown in Figure 5a below.

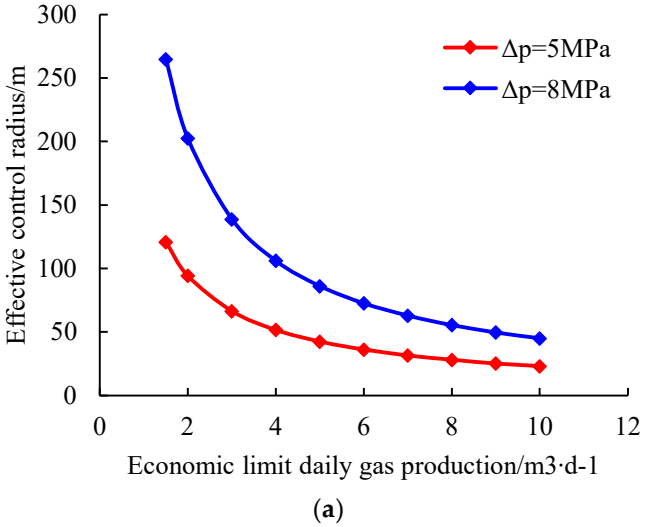

(**a**)

Figure 5. *Cont.*

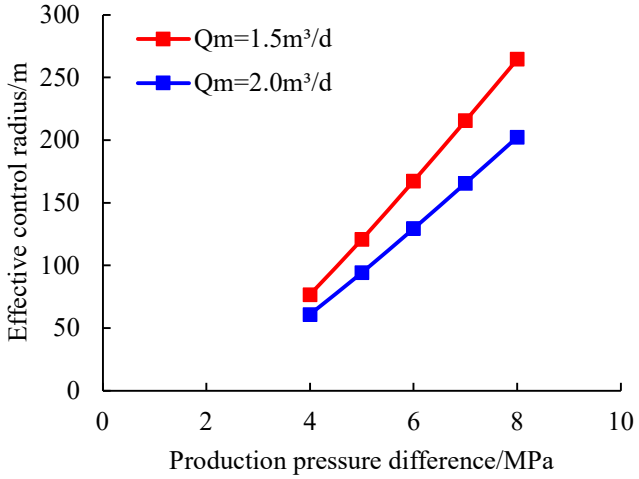

(**b**)

Figure 5. The variation curve of effective control radius under different production conditions. ((**a**) Different economic limits of daily gas production; (**b**) different production pressure differences).

It can be seen from Figure 5a that under certain production pressure differential conditions, the effective control radius of the reservoir gradually decreases with the increase in the economic limit of daily gas production and shows an exponential downward trend. The curves show the same pattern under different production pressure differences. The smaller the production pressure difference is, the smaller the variation range of the effective control radius of the reservoir.

Given a starting pressure gradient of 0.05 MPa·m^{-1}, the relationship between the effective control radius of the reservoir and the production pressure difference is shown in Figure 5b under different economic limits of daily gas production conditions.

As can be seen from Figure 5b, under certain economic limits of daily gas production conditions, the effective control radius of the reservoir gradually increases with the increase in the production pressure differential, and the linear relationship between the two is basically satisfied. When the economic limit of daily gas production is reduced, the demand for the production pressure difference is reduced, and only a lower production pressure difference is needed to achieve the same effective control radius of the reservoir.

The above analysis is carried out under the premise that the physical property of the reservoir is unchanged, and the physical property of the reservoir has a crucial influence on the law of seepage in the reservoir.

The starting pressure gradient of a reservoir is a form of reservoirs' physical properties. There is a functional relationship between the starting pressure gradient of a low-permeability tight sandstone gas reservoir and its fluidity. According to previous studies, the logarithmic relationship between starting pressure gradient G and mobility K/μ is satisfied, which can be expressed as [27]:

$$\ln G = A \cdot \ln\left(\frac{K}{\mu}\right) + B \tag{20}$$

Given the economic limit of daily gas production of 1.5 m^3·d^{-1}, the relationship between the effective control radius of the reservoir and the starting pressure gradient under different production pressure differential conditions is shown in Figure 6a below.

As can be seen from Figure 6a, under certain production pressure differential conditions, the effective control radius of the reservoir gradually decreases with the increase in the starting pressure gradient, and the relationship between the two presents a power function. Under certain starting pressure gradient conditions, there is an obvious change trend between the effective control radius and production pressure difference, and the greater the production pressure difference, the greater the effective control radius of the reservoir.

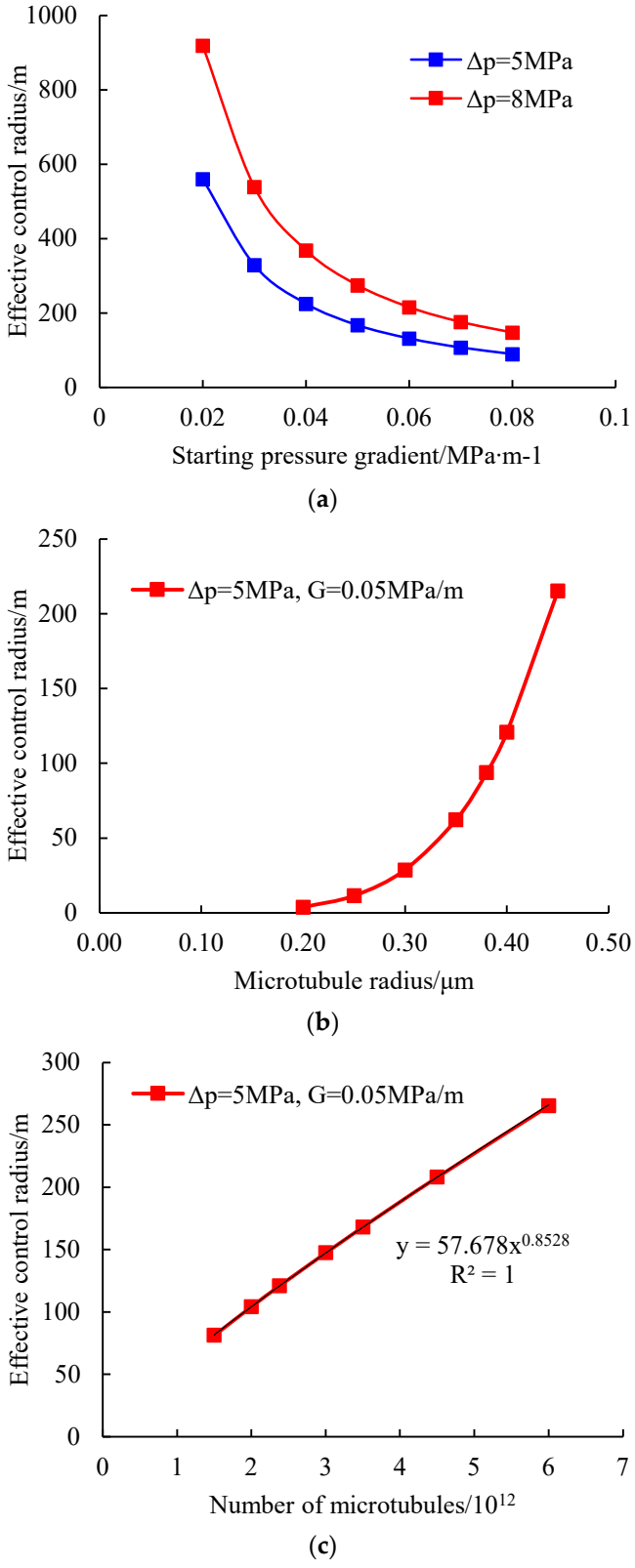

Figure 6. The variation curve of effective control radius under different physical conditions. ((**a**) Different starting pressure gradients; (**b**) different microtubule radiuses; (**c**) different number of microtubules).

In the theoretical model presented in this paper, the reservoir's physical properties are mainly reflected in the microtubule radius R and the number of microtubules N, both of which have important effects on the permeability and porosity of the reservoir. The

influences of these two parameters on the effective control radius of the reservoir are analyzed respectively.

Given that the production pressure difference is 5 MPa, the starting pressure gradient is 0.05 MPa·m^{-1}, and the economic limit of daily gas production is 1.5 m^3·d^{-1}, the relationship between the effective control radius of the reservoir and the microtubule radius is shown in Figure 6b under the condition of a certain number of microtubules.

As can be seen from Figure 6b, under the condition of a certain number of microtubules, both porosity and permeability of the reservoir increase with the increase in the microtubule radius, the effective control radius of the reservoir gradually increases, and the exponential power relationship between the two accords with "concave". When the microtubule radius is reduced to a certain extent, the effective control radius of the reservoir becomes very small, which indicates that when the porosity and permeability drop to a certain value, the gas in the reservoir will be difficult to use, and the seepage will be difficult.

Similarly, given that the production pressure difference is 5 MPa, the starting pressure gradient is 0.05 MPa·m^{-1}, and the economic limit of daily gas production is 1.5 m^3·d^{-1}, the relationship between the effective control radius of the reservoir and the number of microtubules is shown in Figure 6c under the condition that the microtubule radius is certain.

As can be seen from Figure 6c, under the condition of a certain microtubule radius, the effective control radius of the reservoir increases with the increase in the number of microtubules, and the exponential power relationship between the two is "convex" (that is, the power index is less than 1).

Based on the above analysis, the calculation results of the effective control radius of the Sulige tight sandstone gas reservoir under different production conditions and given reservoir physical properties are shown in Table 2 below.

Table 2. Effective application radius of gas reservoir under different conditions.

Starting Pressure Gradient/MPa·m^{-1}	Economic Limit Daily Gas Production/m^3·d^{-1}	Production Pressure Difference/MPa	Effective Control Radius/m
0.05	1.5	5	121
		8	264.8
	2	5	94.4
		8	202.6

Based on the calculation results in Table 2, the effective development well spacing in different regions of the Sulige gas field can be determined.

4. Recovery Evaluation of Tight Sandstone Gas Reservoirs

According to the definition of recovery efficiency, the gas recovery is:

$$\eta = \frac{G_p}{G} \times 100\% \tag{21}$$

where η is gas recovery, in %; G_p is the cumulative gas production, in 10^4 m^3; and G is the geological reserves, in 10^4 m^3.

For the circular uniform constant pressure boundary formation of equal thickness shown in Figure 2, its geological reserves are:

$$G = \left(\pi r_e^2 - \pi r_w^2\right) h \phi S_g \cdot \frac{T_{sc} Z_{sc} p}{T Z p_{sc}} \tag{22}$$

where S_g is the gas saturation.

The cumulative gas production G_p is calculated from the productivity equation (Equation (14)) in Section 3.

Through Matlab software programming, the output/pressure changes under different conditions can be calculated respectively under two modes of constant pressure difference production and constant flow production.

4.1. Gas Recovery under Different Conditions at a Given Pressure Difference

Based on the productivity equation (Equation (14)), the program's realization of the constant pressure difference production process is as follows:

(1) The parameters and initial conditions were assigned: the external boundary pressure $p_e(0)$ = 30 MPa; bottom-hole flow pressure $p_{wf}(0)$ = 30 MPa; the coefficient $a(0) = \frac{\phi\left(\pi r_e^2 - \pi r_w^2\right)h}{\pi R^2(r_e - r_w)} \frac{T_{sc}Z_{sc}}{TZ\left(\frac{p_e(0)+p_{wf}(0)}{2}\right)p_{sc}} \frac{\pi(R-\delta)^4}{8\mu\left(\frac{p_e(0)+p_{wf}(0)}{2}\right)}$, $b(0) = -\frac{\phi\left(\pi r_e^2 - \pi r_w^2\right)h}{\pi R^2(r_e - r_w)} \frac{T_{sc}Z_{sc}}{TZ\left(\frac{p_e(0)+p_{wf}(0)}{2}\right)p_{sc}} \frac{\pi(R-\delta)^3\sigma\cos\theta}{3\mu\left(\frac{p_e(0)+p_{wf}(0)}{2}\right)(r_e - r_w)}$ (viscosity μ and deviation factor Z are functions of average pressure $p = (p_e + p_{wf})/2$); the cumulative gas production $G_p(0) = 0$; and gas recovery $\eta(0) = 0$.

(2) For constant pressure difference production, production pressure difference $\Delta p = p_e - p_{wf}$ was a fixed value. Keeping p_e unchanged before the bottom hole flow pressure p_{wf} could drop to p_e-Δp, p_{wf} was adjusted to the 0.5 MPa drop interval. The flow rate Q_{sc} was obtained by calculating Equation (14), and gas recovery was calculated using the definition (Equation (21)).

$$\frac{a(i)Q_{sc}(i)}{b(i)^2}\ln^{\frac{b(i)p_e(i)-Q_{sc}(i)}{b(i)p_{wf}(i)-Q_{sc}(i)}} + \frac{a(i)}{b(i)}\left[p_e(i) - p_{wf}(i)\right] + (r_e - r_w) = 0$$

$$\eta(i) = \frac{G_p(i)}{G} \times 100\%$$

(3) When the bottom-hole flow pressure p_{wf} dropped to $p_e - \Delta p$, pe and p_{wf} simultaneously dropped at an interval of 0.5 MPa to keep the pressure difference Δp unchanged, and the flow rate Q_{sc} was calculated by Equation (14) as in step (2).

(4) The cycle was followed until the termination condition was reached (p_{wf} reached the abandonment pressure).

The production process of constant pressure difference under different production pressure differences was simulated to obtain the variation curves of gas recovery with time and bottom-hole flow pressure (Figure 7a,b), and the relationship between the ultimate gas recovery and production pressure difference was fitted, as shown in Figure 7c.

It can be seen from Figure 7a,b that under constant pressure differential production, the greater the production pressure differential, the faster the bottom-hole flow pressure drop, the shorter the time required to reach the abandoned bottom-hole pressure, and the corresponding recovery degree, that is, the smaller the gas recovery. When the production pressure difference is 3 MPa, 5 MPa, 8 MPa, 12 MPa, and 15 MPa, the ultimate gas recovery after reaching the abandoned bottom-hole pressure is 75.18%, 71.40%, 65.78%, 58.42%, and 53.01%, respectively. As can be seen from Figure 7c, the ultimate gas recovery after reaching the abandoned bottom-hole pressure decreases with the increase in the production pressure difference, and the relationship between the two basically satisfies the linear function.

Under the condition of constant reservoir physical properties, given a production pressure difference of 5 MPa, the change curve of gas recovery with bottom-hole flow pressure was simulated (Figure 8a), and the relationship curve between ultimate gas recovery and abandoned bottom-hole pressure was fitted, as shown in Figure 8b.

As can be seen from Figure 8a, under the condition that the production pressure difference is 5 MPa, the corresponding gas recovery gradually decreases with the increase in the abandoned bottom-hole pressure. When the abandoned bottom-hole pressure is 3 MPa, 5 MPa, 8 MPa, 10 MPa, and 12 MPa, the ultimate gas recovery is 78.98%, 71.40%, 60.25%, 53.01%, and 45.98%, respectively, and the relationship between the ultimate gas recovery and the abandoned bottom-hole pressure basically presents a linear function (Figure 8b).

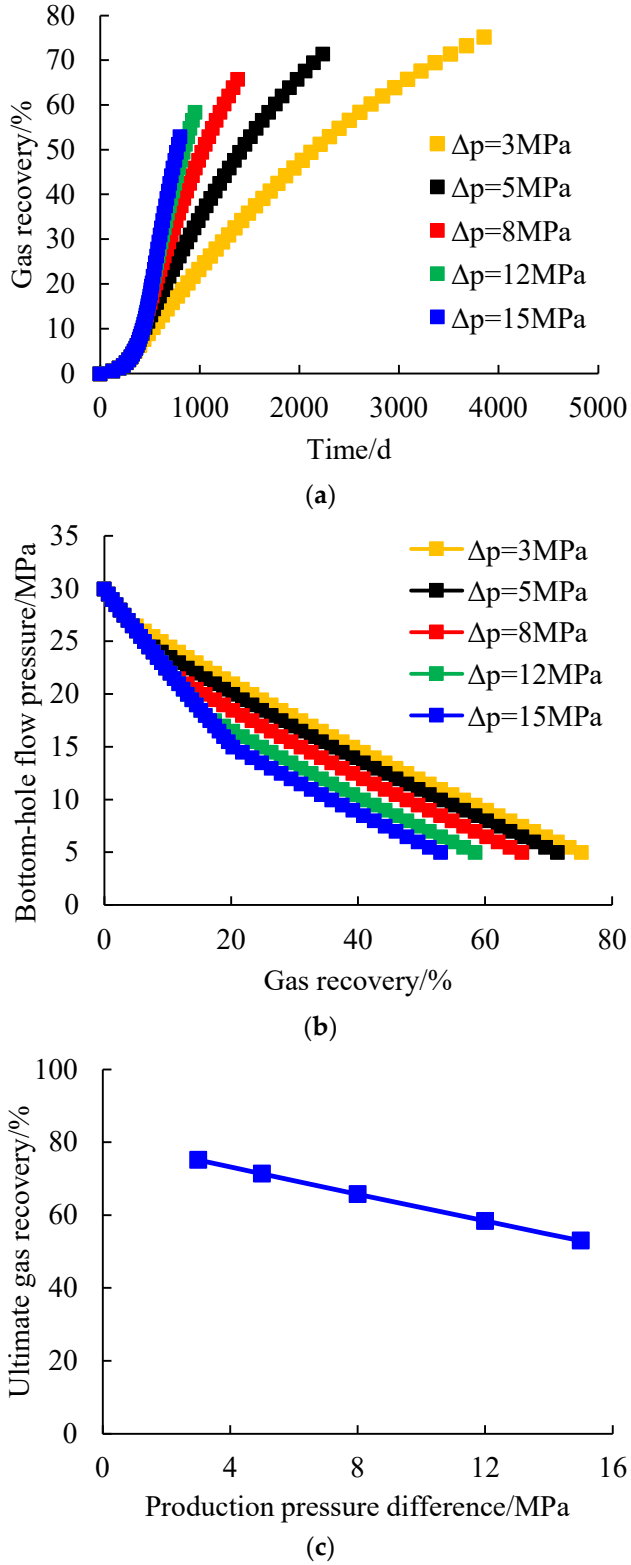

Figure 7. The variation curve of gas recovery at different production pressure differences. ((**a**) The variation curve of gas recovery over time; (**b**) the variation curve of gas recovery with bottom-hole flow pressure; (**c**) the curve of the relationship between ultimate gas recovery and production pressure difference).

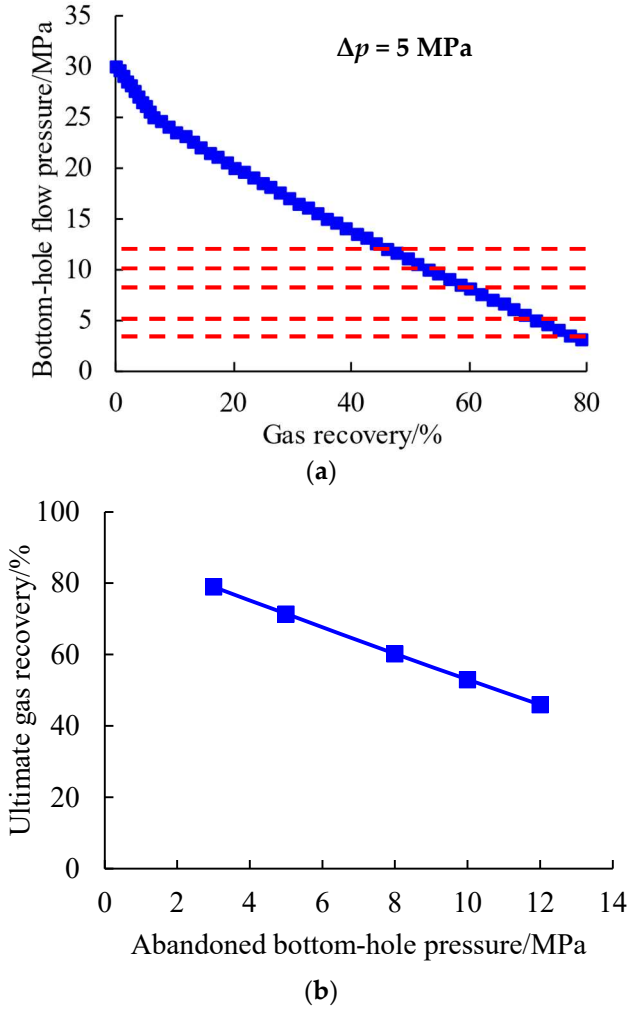

Figure 8. The variation curve of gas recovery at different abandoned bottom-hole pressure when Δp = 5 MPa. ((**a**) The variation curve of gas recovery with bottom hole flowing pressure; (**b**) the curve of the relationship between ultimate gas recovery and abandoned bottom-hole pressure).

The size of the single-well control radius is the standard to measure the recoverable reserves of a gas well. A larger single-well control radius means more reservoir reserves can be utilized by a gas well. Under the condition that the reservoir's physical properties and reservoir radius remain unchanged, the production pressure difference is 5 MPa, and the change curves of gas recovery with time and bottom-hole flow pressure under different ratios of the control radius were simulated (Figure 9a,b). The relationship curves between the ultimate gas recovery and the ratio of control radius were fitted, as shown in Figure 9c.

As can be seen from Figure 9a,b, under the condition that the production pressure difference is 5 MPa, the smaller the control radius of a single well, the smaller its ratio to the reservoir radius, the faster the bottom-hole flow pressure drops, and the smaller the gas recovery under the same bottom-hole flow pressure. When the ratio of the control radius is 0.33, 0.50, 0.67, 0.83, and 1.00, the ultimate recovery rate of gas reservoir is 23.78%, 35.69%, 47.59%, 59.49%, and 71.40%, respectively. As can be seen from Figure 9c, the ultimate gas recovery after reaching the abandoned bottom-hole pressure increases with the increase in the ratio of the control radius, and the relationship between the two is in line with a linear function.

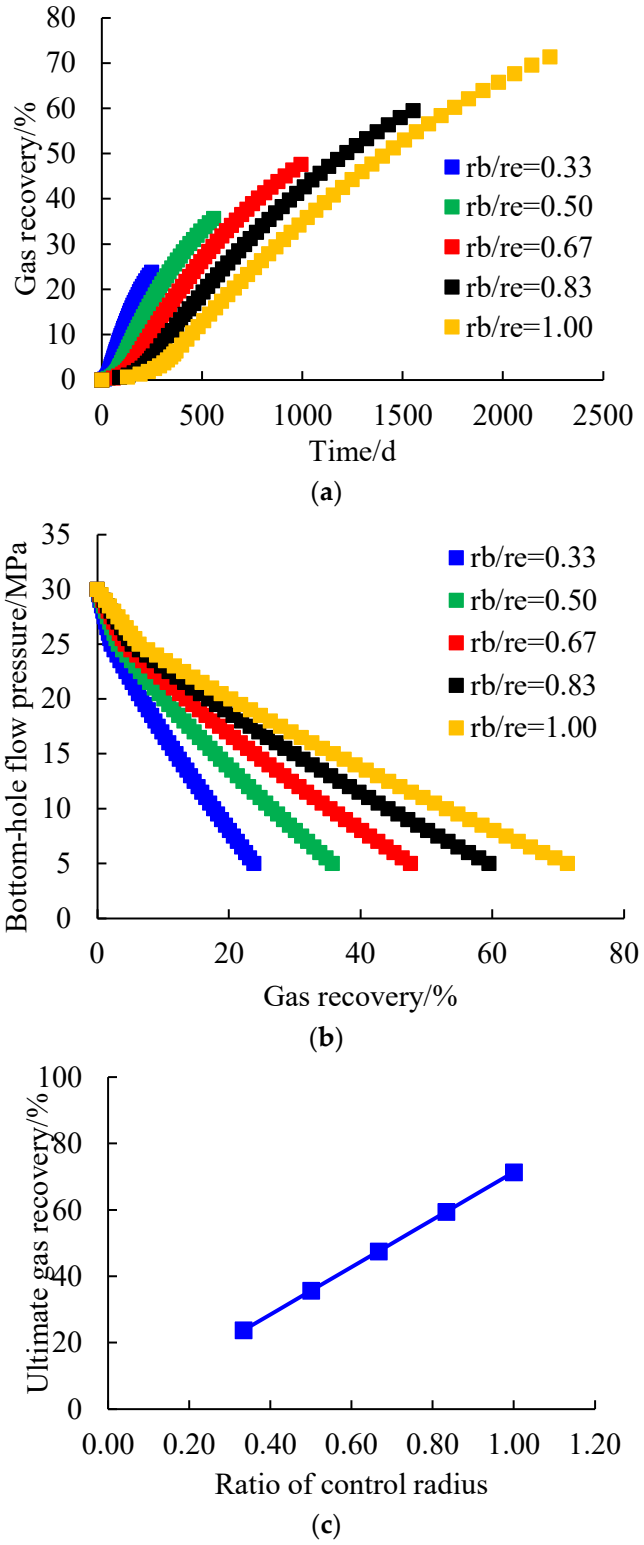

Figure 9. The variation curve of gas recovery at different ratios of the control radius when Δp = 5 MPa. ((**a**) The curve of gas recovery over time; (**b**) the variation curve of gas recovery with bottom-hole flow pressure; (**c**) the curve of the relationship between the ultimate gas recovery and the ratio of the control radius).

Reservoir quality index (RQI) is a characteristic parameter that reflects the change in the microscopic pore structure and is an embodiment of a reservoir's physical properties. The reservoir quality index is defined as [28]:

$$RQI = \sqrt{\frac{K}{\phi}} \tag{23}$$

Given that the production pressure difference is 5 MPa, the variation curves of bottom-hole flow pressure and gas recovery with time under different reservoir quality indexes were simulated, as shown in Figure 10a,b.

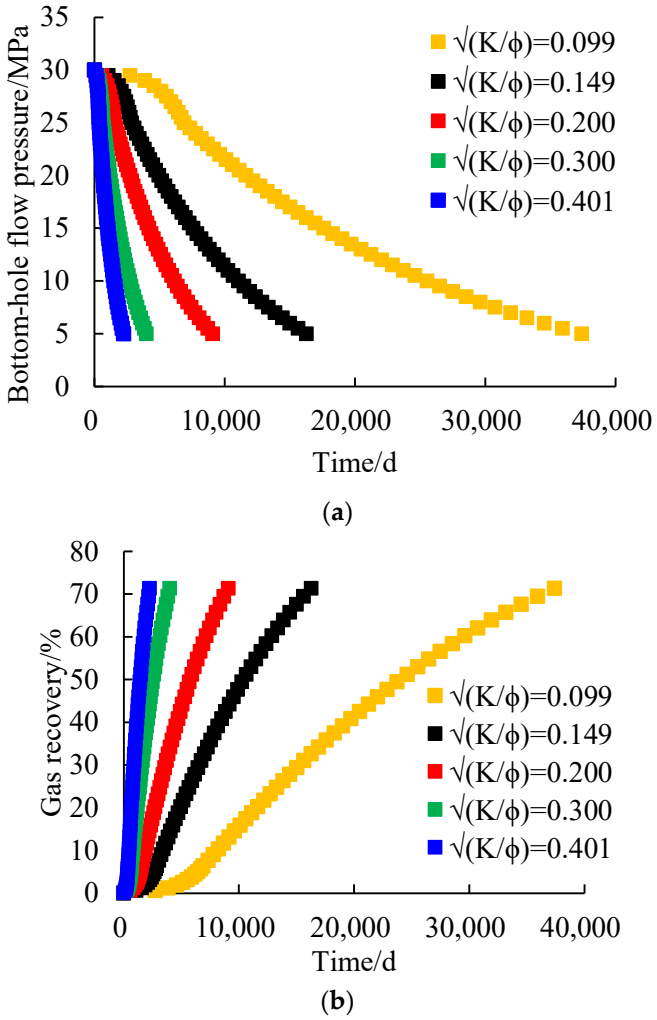

Figure 10. The variation curve of gas recovery at different reservoir quality indexes when Δp = 5 MPa. ((**a**) The curve of bottom-hole flow pressure over time; (**b**) the curve of gas recovery over time).

It can be seen from Figure 10a,b that reservoirs with different reservoir quality indexes have the same ultimate gas recovery after production reaches abandoned bottom-hole pressure, but the time required is different. The larger the reservoir quality index is, the faster the bottom-hole flow pressure drops, and the shorter the time required to reach abandoned bottom-hole pressure.

4.2. Gas Recovery under Different Conditions at a Given Production Rate

Based on the productivity equation (Equation (14)), the program's realization of the production process with a fixed production rate was as follows:

(1) As with the production of the constant pressure difference, the parameters and initial conditions were preassigned: the external boundary pressure $p_e(0)$ = 30 MPa; bottom-hole flow pressure $p_{wf}(0)$ = 30 MPa; the coefficient $a(0) = \frac{\phi\left(\pi r_e^2 - \pi r_w^2\right)h}{\pi R^2(r_e - r_w)} \frac{T_{sc}Z_{sc}}{TZ\left(\frac{p_e(0)+p_{wf}(0)}{2}\right)p_{sc}} \frac{\pi(R-\delta)^4}{8\mu\left(\frac{p_e(0)+p_{wf}(0)}{2}\right)}$, $b(0) = -\frac{\phi\left(\pi r_e^2 - \pi r_w^2\right)h}{\pi R^2(r_e - r_w)} \frac{T_{sc}Z_{sc}}{TZ\left(\frac{p_e(0)+p_{wf}(0)}{2}\right)p_{sc}} \frac{\pi(R-\delta)^3\sigma\cos\theta}{3\mu\left(\frac{p_e(0)+p_{wf}(0)}{2}\right)(r_e - r_w)}$ (viscosity μ and deviation factor Z are functions of average pressure $p = (p_e + p_{wf})/2$); the cumulative gas production $G_p(0) = 0$; and gas recovery $\eta(0) = 0$.

(2) Production starting point: Q_{sc} is a fixed value. Assuming that the starting point (point 1) p_e is unchanged, that is, $p_e(1)$ = 30 MPa, then the average pressure $p(1) = (p_e(1) + p_{wf}(1))/2 = (30 + p_{wf}(1))/2$. Viscosity $\mu(1)$ and deviation factor $Z(1)$ are functions of average pressure $p(1)$, coefficients $a(1)$ and $b(1)$ are functions of the viscosity and deviation factor, so $a(1)$ and $b(1)$ are functions of the average pressure $p(1)$. $p_{wf}(1)$ was calculated by Equation (14), and gas recovery was calculated by Equation (21).

$$\frac{a(1)Q_{sc}}{b(1)^2}\ln\frac{b(1)p_e(1)-Q_{sc}}{b(1)p_{wf}(1)-Q_{sc}} + \frac{a(1)}{b(1)}\left[p_e(1) - p_{wf}(1)\right] + (r_e - r_w) = 0$$

$$\eta(1) = \frac{G_p(1)}{G} \times 100\%$$

(3) Point 2: Assigning $\omega \cdot p_e(1) + (1 - \omega) \cdot p_{wf}(1)$ (ω is the scale coefficient) to $p_e(2)$, $p_{wf}(2)$ was calculated from Equation (14).

(4) The cycle was followed until the termination condition was reached (p_{wf} reached the abandonment pressure).

$$p_e(i) = \omega \cdot p_e(i-1) + (1-\omega)p_{wf}(i-1)$$

$$\frac{a(i)Q_{sc}}{b(i)^2}\ln\frac{b(i)p_e(i)-Q_{sc}}{b(i)p_{wf}(i)-Q_{sc}} + \frac{a(i)}{b(i)}\left[p_e(i) - p_{wf}(i)\right] + (r_e - r_w) = 0$$

$$\eta(i) = \frac{G_p(i)}{G} \times 100\%$$

The variation curves of gas recovery with time and bottom-hole flow pressure (Figure 11a,b) were obtained by simulating the production process at a given production rate under different daily gas production limits, and the relationship between the ultimate gas recovery and daily gas production was fitted, as shown in Figure 11c.

It can be seen from Figure 11a,b that at a fixed production rate, the higher the daily gas production, the faster the bottom-hole flow pressure drops, the shorter the time required to reach the abandoned bottom-hole pressure, and the smaller the corresponding gas recovery. When the daily gas production is 0.25×10^4 $m^3 \cdot d^{-1}$, 0.50×10^4 $m^3 \cdot d^{-1}$, 0.75×10^4 $m^3 \cdot d^{-1}$, 1.00×10^4 $m^3 \cdot d^{-1}$, and 1.10×10^4 $m^3 \cdot d^{-1}$, the ultimate gas recovery after reaching the abandoned bottom-hole pressure is 78.85%, 77.13%, 75.58%, 74.09%, and 73.47%, respectively. As can be seen from Figure 11c, the ultimate gas recovery after reaching the abandoned bottom-hole pressure decreases with the increase in daily gas production, and the relationship between the two basically satisfies the linear function.

Under the condition of constant reservoir physical properties and given daily gas production of 1.10×10^4 $m^3 \cdot d^{-1}$, the variation curve of gas recovery with bottom-hole flow pressure was simulated (Figure 12a), and the relationship curve between the ultimate gas recovery and abandoned bottom-hole pressure was fitted, as shown in Figure 12b.

As can be seen from Figure 12a, under the condition of daily gas production of 1.10×10^4 $m^3 \cdot d^{-1}$, the corresponding gas recovery gradually decreased with the increase in abandoned bottom-hole pressure. When the abandoned bottom-hole pressure is 3 MPa, 5 MPa, 8 MPa, 10 MPa, and 12 MPa, the ultimate gas recovery is 78.93%, 73.47%, 64.09%, 57.48%, and 50.81%, respectively. The relationship between the ultimate gas recovery and the abandoned bottom-hole pressure basically presents a linear function (Figure 12b).

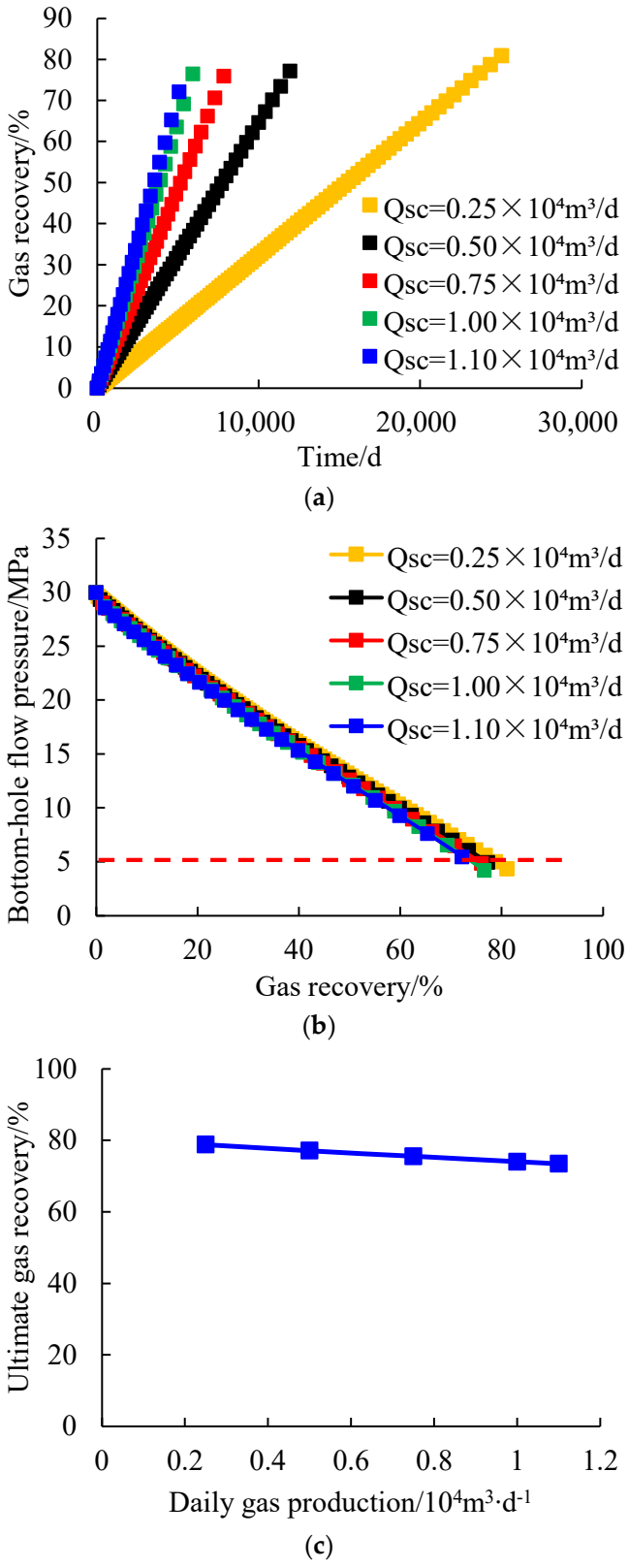

Figure 11. The variation curve of gas recovery at different daily gas production limits. ((**a**) The variation curve of gas recovery over time; (**b**) the variation curve of gas recovery with bottom-hole flow pressure; (**c**) the curve of the relationship between ultimate gas recovery and daily gas production).

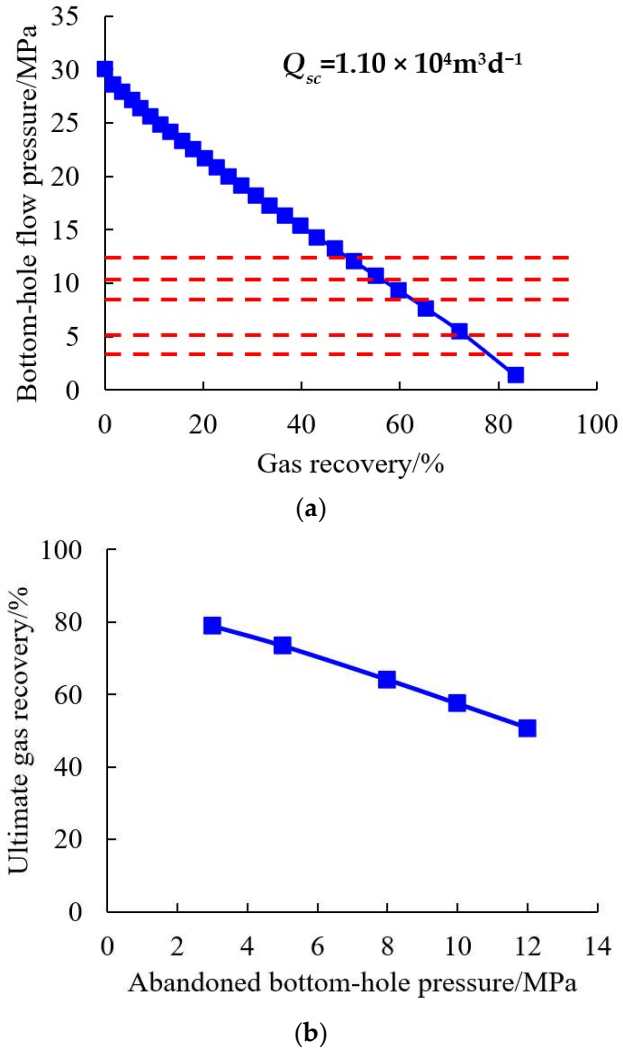

Figure 12. The variation curve of gas recovery at different abandoned bottom-hole pressures when Q_{sc} = 1.10 × 10^4 $m^3 \cdot d^{-1}$. ((**a**) The variation curve of gas recovery with bottom hole flowing pressure; (**b**) the curve of the relationship between ultimate gas recovery and abandoned bottom-hole pressure).

With the same reservoir physical properties and reservoir radius, given daily gas production of 1.10 × 10^4 $m^3 \cdot d^{-1}$, the variation curve of gas recovery with bottom-hole flow pressure under different ratios of the control radius was simulated (Figure 13a), and the relationship curve between the ultimate gas recovery and the ratio of the control radius was fitted, as shown in Figure 13b.

As can be seen from Figure 13a, under the condition of daily gas production of 1.10 × 10^4 $m^3 \cdot d^{-1}$, the smaller the control radius, the smaller the ratio to the reservoir radius, the faster the bottom-hole flow pressure drops, and the smaller the gas recovery under the same bottom-hole flow pressure. When the ratio of the control radius is 0.33, 0.50, 0.67, 0.83, and 1.00, the ultimate gas recovery is 8.48%, 19.11%, 34.00%, 53.14%, and 76.55%, respectively. As can be seen from Figure 13b, the ultimate gas recovery after reaching the abandoned bottom-hole pressure increases with the increase in the ratio of the control radius, and the relationship between the two conforms to the power function relationship.

Given the daily gas production of 1.10 × 10^4 $m^3 \cdot d^{-1}$, the variation curve of gas recovery with bottom-hole flow pressure under different reservoir quality indexes was simulated (Figure 14a), and the relationship curve between the ultimate gas recovery and reservoir quality index was fitted, as shown in Figure 14b.

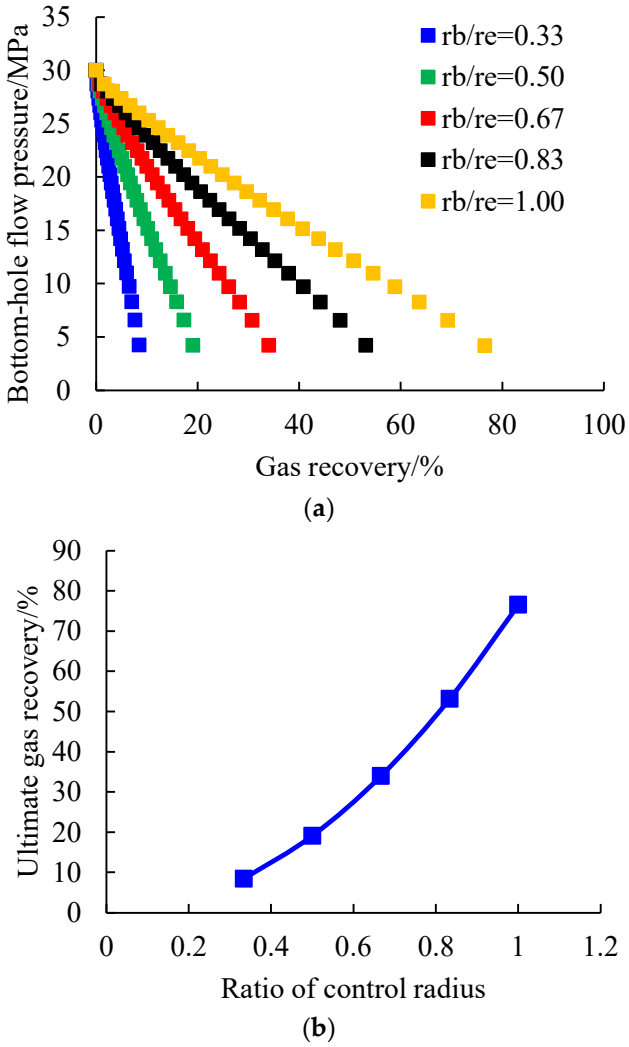

Figure 13. The variation curve of gas recovery at different ratios of the control radius when Q_{sc} = 1.10 × 10^4 $m^3 \cdot d^{-1}$. ((**a**) The variation curve of gas recovery with bottom-hole flow pressure; (**b**) the curve of the relationship between the ultimate gas recovery and the ratio of control radius).

As can be seen from Figure 14a, under the condition of daily gas production of 1.10 × 10^4 $m^3 \cdot d^{-1}$, the smaller the reservoir quality index is, the faster the bottom-hole flow pressure drops, and the shorter the time required to reach the abandoned bottom-hole pressure. When the reservoir quality index is 0.099, 0.149, 0.200, 0.300, and 0.401, the ultimate gas recovery is 61.64%, 70.22%, 74.03%, 77.46%, and 78.85%, respectively. As can be seen from Figure 14b, there is a nonlinear relationship between the ultimate gas recovery and the reservoir quality index. With the increase in the reservoir quality index, the ultimate gas recovery first increases rapidly and then slows, and there is an obvious critical permeability (0.1 mD).

4.3. Application Example

The Su75 well is located in the north of the western Sulige gas field, with a block area of 989 km^2. The ancient strata in the Su75 block include the Benxi Formation, Taiyuan Formation, Shanxi Formation, Shihezi Formation, and Shiqianfeng Formation from the bottom up. The main gas-bearing formations in the area are He-8 Member and Shan-1 Member; in addition, there are the Taiyuan Formation, Shan-2 Member, and other formations. The reservoir porosity ranges from 5.02% to 19.91%, with an average value of 8.91%. Permeability ranges from 0.005 to 14.726 mD, with an average of 0.077 mD. The

original gas saturation of the He-8 Member is 62.3%, that of the Shan-1 Member is 59%. The original formation pressure was 29.22 MPa in the He-8 Member and 29.56 MPa in the Shan-1 Member.

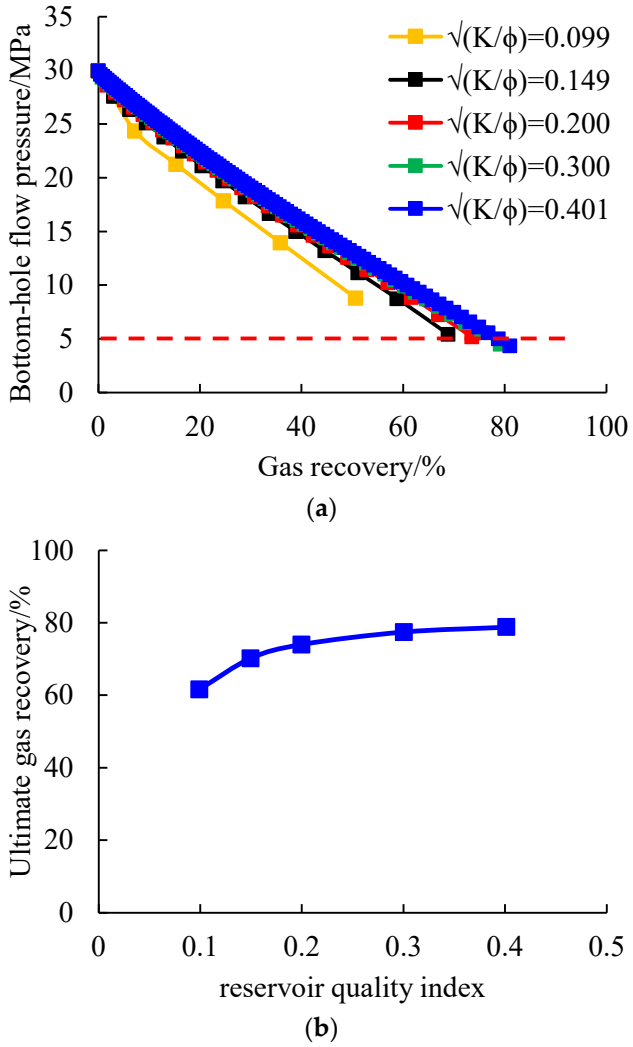

Figure 14. The variation curve of gas recovery at different reservoir quality indexes when Q_{sc} = 1.10 × 10^4 $m^3 \cdot d^{-1}$. ((**a**) The variation curve of gas recovery with bottom-hole flow pressure; (**b**) the curve of the relationship between ultimate gas recovery and reservoir quality index).

For a select production well in the Su75 well area of the Sulige gas field, the basic geological information is shown in Table 3.

Table 3. Geological information table of production gas well in Su75 well area.

Pound Sign	Position	Depth/m	Thickness/m	Average Porosity/%	Average Gas Saturation/%	Average Permeability/mD	Control Reserves/10^4 m^3
SX-1	He-8 Member	3625.0	17.0	14.81	47.91	1.45	6366.84

The actual production data of the well (Figure 15) were used to simulate and calculate the change curve of the recovery efficiency, and the results are shown in Figure 16.

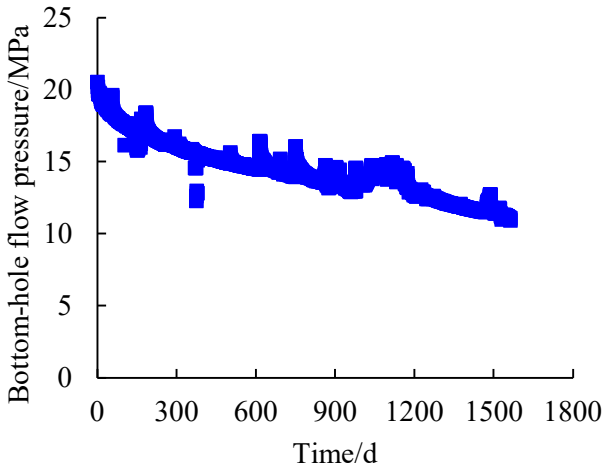

Figure 15. The variation curve of bottom-hole flow pressure with time in the actual production process of well SX-1.

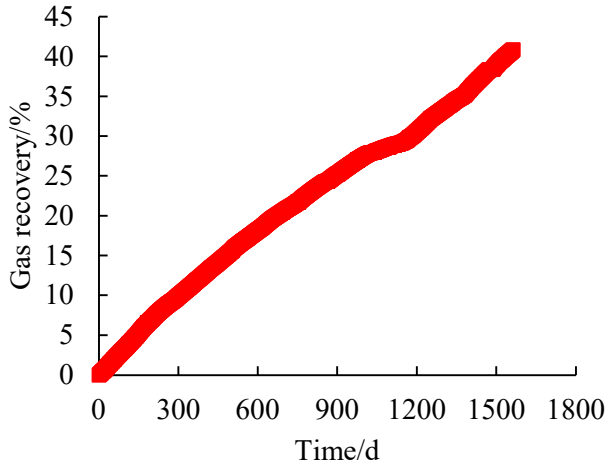

Figure 16. The variation curve of gas recovery with time of well SX-1.

As can be seen from Figure 16, the final recovery rate of well SX-1 based on the production data simulation calculation is 40.88%.

5. Conclusions

(1) Based on Newton's law of motion, the steady-state model of gas–water two-phase seepage was derived by mechanical analysis considering the displacement force, capillary force, wall friction force, and internal friction force, and the productivity equation was established on this basis.

(2) The calculation method for the effective control radius of a tight sandstone gas reservoir was established based on the steady-state model of gas–water two-phase seepage. The results show that the effective control radius of the reservoir decreases with the increase in the economic limit of daily gas production, increases with the increase in the production pressure difference, slightly decreases with the increase in the starting pressure gradient, and increases with the increase in the microtubule radius and microtubule number.

(3) The calculation of gas recovery under two modes of constant pressure difference and constant production rate was realized using Matlab software programming. The calculation results show that gas recovery decreases with the increase in the production pressure difference and abandoned bottom-hole pressure and increases with the increase in the ratio of the control radius. Under a constant pressure difference

production, gas recovery with a different reservoir quality index is the same, while under a constant production rate, gas recovery first increases rapidly and then slowly with the increase in the reservoir quality index, and there is an obvious critical permeability (0.1 mD). Finally, a production well in the Su75 well area of the Sulige gas field was selected, and gas recovery was 40.88% based on the actual production data.

Author Contributions: Methodology, S.G.; Software, H.L.; Validation, W.X.; Investigation, L.Y.; Resources, W.Z.; Data curation, D.H.; Writing—original draft, J.Z.; Writing—review & editing, B.L.; Project administration, W.A. All authors have read and agreed to the published version of the manuscript.

Funding: This research received no external funding.

Data Availability Statement: Data is contained within the article.

Conflicts of Interest: The authors declare no conflict of interest.

References

1. Hao, Y.; Xu, M.; Xu, X. Correct calculation of dynamic reserves of low permeability gas reservoirs. *Pet. Explor. Dev.* **2002**, *5*, 66–68.
2. Li, B.; Shi, W.; Wang, S.; Hao, Y. Discussion on the problems in the calculation of gas field recovery efficiency. *Offshore Oil* **2006**, *3*, 55–60.
3. Li, S. *Natural Gas Engineering*; Petroleum Industry Press: Beijing, China, 2000.
4. Huang, B.; Liu, S.; Tang, H. *Gas Reservoir Engineering and Dynamic Analysis Method*; Petroleum Industry Press: Beijing, China, 2004.
5. Farouk, S.; Sen, S.; Ahmad, F.; Al-Kahtany, K.; Benmamar, S.; Abdeldaim, A. Assessment of pore pressure in the Oligocene–Pleistocene stratigraphy of the West Delta Deep Marine, offshore Nile Delta, Egypt. *Mar. Geophys. Res.* **2024**, *45*, 6. [CrossRef]
6. Farouk, S.; Sen, S.; Pigott, J.D.; Sarhan, M.A. Reservoir characterization of the middle Miocene Kareem sandstones, Southern Gulf of Suez Basin, Egypt. *Geomech. Geophys. Geo-Energ. Geo-Resour.* **2022**, *8*, 130. [CrossRef]
7. Zhang, L.; Sun, J. Methods and approaches to enhance gas reservoir recovery. *Nat. Gas Ind.* **1992**, *5*, 7+32–36.
8. Chen, S.; Zhang, N.; Liu, J.; Chen, S. Discussion on enhancing oil recovery from late development of Carboniferous gas reservoirs in eastern Sichuan. *Nat. Gas Ind.* **2009**, *29*, 92–94+143.
9. Wu, S. Analysis of recovery efficiency calculation method for low permeability gas reservoir. *Neijiang Technol.* **2012**, *33*, 16.
10. Hao, Y. Calculation of recovery efficiency of low permeability gas reservoir. *Low Permeability Oil Gas Field* **1998**, *4*, 39–45.
11. Zhu, Y.; Liu, J.; Zhang, G.; Zhu, D.; Li, J. Comparative analysis of gas well production decline law analysis methods. *Nat. Gas Explor. Dev.* **2009**, *32*, 28–31.
12. Li, Z.; Hao, Y. Revision of volumetric method for calculating gas reservoir recovery and recoverable reserves. *Nat. Gas Ind.* **2001**, *21*, 71–74.
13. Guo, P.; Zhang, M.; Huang, Q.; Liu, Q. *Research on Development Mechanism of Low Permeability Tight Sandstone Gas Reservoir*; Petroleum Industry Press: Beijing, China, 2009; pp. 178–179.
14. Sun, H.; Wang, Z.; Bai, J.; Chen, W. Analysis on horizontal well development effect of Xujiahe Formation gas reservoir in central Sichuan. *Oil Drill. Prod. Technol.* **2010**, *32*, 118–119.
15. Zhang, Y. Optimization analysis of fracture parameters of fractured horizontal Wells in gas reservoirs. *Sci. Technol. Eng.* **2010**, *10*, 2861–2864.
16. Dong, S.; Guo, J.; Guo, Z.; Meng, D.; Ji, G.; Cheng, L. Evaluation of remaining reserves and strategies for enhancing oil recovery in Su 6 block. *Fault-Block Oil Gas Field* **2020**, *27*, 74–79.
17. Hu, Y.; Mei, Q.; Wang, J.; Che, Y.; Xu, X. Optimization of well pattern filling in tight sandstone gas reservoirs. *Nat. Gas Geosci.* **2020**, *31*, 1326–1333.
18. Guo, S.; Li, Z.; Zhang, G.; Liu, Y. Research on Enhanced oil recovery strategies of Songnan developed gas field. In Proceedings of the 32nd National Natural Gas Academic Conference, Chongqing, China, 12 November 2020; pp. 750–754. [CrossRef]
19. Xu, Y.; Zhang, B.; Liu, Q.; Luo, Y. Research on late optimization and adjustment scheme of surface gathering and transportation system of old gas field. *Pet. Plan. Des.* **2017**, *28*, 16–19.
20. Wen, Q.; Zhang, W.; Liu, Z. Study on optimization model of ground system adjustment and renovation in middle and late stage of old gas field. *Yunnan Chem. Ind.* **2020**, *47*, 185–186.
21. Han, F.; Li, R.; Li, G.; Dai, X.; Chen, S. Drilling technology of small hole horizontal well in tight sand conglomerate gas reservoir of Qingshen Gas field. *Oil Drill. Technol.* **2013**, *41*, 56–61.
22. Zhang, T.; Li, Y.; Sun, S.; Bai, H. Accelerating flash calculations in unconventional reservoirs considering capillary pressure using an optimized deep learning algorithm. *J. Pet. Sci. Eng.* **2020**, *195*, 107886. [CrossRef]
23. Xie, H.; Tian, S.; Zhao, D.; Qu, J. Application of starting pressure gradient in low permeability reservoir development. *Nat. Gas Explor. Dev.* **2008**, *2*, 28–31+78.
24. Wang, D.; Li, Z.; Zhao, J.; He, Y.; Hao, F. Theory and application of advanced water injection in low permeability reservoir. *Acta Pet. Sin.* **2007**, *6*, 78–81+86.

25. Su, Y.; Chen, M. Study on effective production law of low permeability pressure sensitive reservoir. *J. Shaanxi Univ. Sci. Technol. (Nat. Sci. Ed.)* **2015**, *33*, 104–110.
26. Zhu, W.; Liu, J.; Song, H.; Sun, Y.; Wang, M. Calculation method for effective production of non-Darcy percolation in low/ultra-low permeability reservoirs. *Acta Pet. Sin.* **2010**, *31*, 452–457.
27. Deng, Y.; Liu, H. Starting pressure gradient test of oil-water two-phase seepage in low permeability core. *Oil Drill. Prod. Technol.* **2006**, *28*, 37–40.
28. Zeng, J.; Bai, S.; Li, H.; Wang, J. Productivity prediction method based on low permeability reservoir quality evaluation. *J. Yangtze Univ.* **2017**, *14*, 5–6+40–44.

Disclaimer/Publisher's Note: The statements, opinions and data contained in all publications are solely those of the individual author(s) and contributor(s) and not of MDPI and/or the editor(s). MDPI and/or the editor(s) disclaim responsibility for any injury to people or property resulting from any ideas, methods, instructions or products referred to in the content.